Chinese Journal of Mechanical Engineering: Additive Manufacturing Frontiers 1 (2022) 100018

Contents lists available at ScienceDirect

Chinese Journal of Mechanical Engineering: Additive Manufacturing Frontiers

journal homepage: www.elsevier.com/locate/cjmeamf

Challenges in the Technology Development for Additive Manufacturing in Space

Andrea Zocca[a], Janka Wilbig[a], Anja Waske[a], Jens Günster[a,*], Martinus Putra Widjaja[a], Christian Neumann[b], Mélanie Clozel[b], Andreas Meyer[b], Jifeng Ding[c], Zuoxin Zhou[c], Xiaoyong Tian[d]

[a] BAM Bundesanstalt für Materialforschung und -prüfung, Berlin, 12203, Germany
[b] Institut für Materialphysik im Weltraum, Deutsches Zentrum für Luft- und Raumfahrt (DLR), 51170 Köln, Germany
[c] Beijing Space Vehicle General Design Department, CAST, Beijing, 100094, China
[d] State Key Laboratory for Manufacturing System Engineering, Xi'an Jiaotong University, Xi'an, 710049, China

ARTICLE INFO

Keywords:
Zero-g
Microgravity
Additive manufacturing
Regolith
Steel
Fiber
PEEK

ABSTRACT

Instead of foreseeing and preparing for all possible scenarios of machine failures, accidents, and other challenges arising in space missions, it appears logical to take advantage of the flexibility of additive manufacturing for "in-space manufacturing" (ISM). Manned missions into space rely on complicated equipment, and their safe operation is a great challenge. Bearing in mind the absolute distance for manned missions to the Moon and Mars, the supply of spare parts for the repair and replacement of lost equipment via shipment from Earth would require too much time. With the high flexibility in design and the ability to manufacture ready-to-use components directly from a computer-aided model, additive manufacturing technologies appear to be extremely attractive in this context. Moreover, appropriate technologies are required for the manufacture of building habitats for extended stays of astronauts on the Moon and Mars, as well as material/feedstock. The capacities for sending equipment and material into space are not only very limited and costly, but also raise concerns regarding environmental issues on Earth. Accordingly, not all materials can be sent from Earth, and strategies for the use of in-situ resources, i.e., in-situ resource utilization (ISRU), are being envisioned. For the manufacturing of both complex parts and equipment, as well as for large infrastructure, appropriate technologies for material processing in space need to be developed.

1. Introduction

1.1. In-space manufacturing and additive manufacturing (AM)

Considering future human exploration of the Moon or Mars, it is clear that additive manufacturing (AM) will be necessary. For example, if a fast and flexible response to an accident involving the loss or damage of parts is required, sending resupply missions is not an option. This is also the case if there is a demand for special parts that are not in stock. In these situations, "in-space manufacturing" (ISM), i.e., the ability to directly manufacture objects of any type in space, becomes a necessity. Moreover, as an additional advantage of ISM, parts and components do not need to survive the harsh conditions of a rocket launch from Earth. In this context, AM has an advantage in that "ready to use" parts can be manufactured directly from a feedstock material like a filament or powder, and that only as much material as needed is consumed to form the part. Hence, it appears logical to develop AM technologies able to function in microgravity (μg) conditions or at reduced gravity on the Moon and Mars. Once appropriate technologies are developed, the parts can be 3D-printed directly in space. The materials may be carried from Earth or found in space, such as on the Moon and Mars, depending on the mission scenario.

1.2. In-situ resource utilization (ISRU)

For the extension of manned missions to the Moon and Mars, the utilization of in-situ resources must be of the utmost priority, as the capacities for carrying equipment and material into space are not only limited and costly, but also raise concerns regarding environmental issues on Earth. The surfaces of the Moon and Mars are not hospitable owing to radiation, low atmospheric pressure, and/or almost no atmosphere, as well as extreme temperatures and temperature changes. Human survival and safe travel from and to Earth would require artificial habitats. These, in turn, would need to be built from resources existing in these locations, and to include complex life-support systems and a minimum of

* Corresponding author.
E-mail address: jens.guenster@bam.de (J. Günster).

https://doi.org/10.1016/j.cjmeam.2022.100018
Received 8 October 2021; Received in revised form 24 December 2021; Accepted 9 January 2022
Available online 16 February 2022

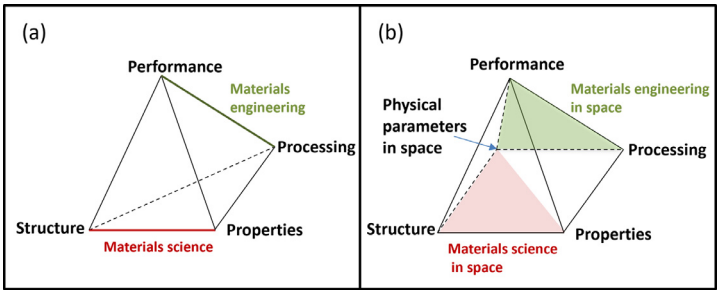

Fig. 1. (a) Structure-process-properties-performance paradigm of materials science and engineering; (b) Adapted paradigm "structure-physics in space-process-properties-performance".

infrastructure. This strategy is called in-situ resource utilization (ISRU). The concept of ISRU envisions the manufacturing of complex parts from abundant materials, such as lunar or Martian regoliths [1].

Whether a material or other item is a resource depends on the availability of appropriate technologies. For example, for transforming abundant materials like regolith into useful structures and parts, sunlight can be concentrated, and the powdery material can be consolidated and shaped into rigid structures. In that sense, technologies can act as a catalyst for creating protective structures for supporting human life in hostile lunar and Martian environments, i.e., by using locally available resources such as material and energy.

For the development of the related strategies, not only the appropriate technologies need to be available; moreover, energy (e.g., solar energy) needs to be harvested, and the materials and their properties need to be known at all stages throughout the entire process chain.

The present communication sheds light on the specific challenges related to ISM and ISRU.

1.3. Manufacturing technology development for space

In AM, the final material properties and manufacturing technologies are more closely related than in most other conventional manufacturing technologies. In AM, the bulk material is created together with the part. The material fed into the process to build up the part is generally called "feedstock," and it comes as a powder, paste, wire, or liquid. In the AM process, it is fused, consolidated, crosslinked, or condensed in a layer-by-layer fashion to form a part. The fact that each part's geometry often significantly influences the material properties makes the complexity of the process evident. In contrast, in conventional manufacturing processes such as metalworking, a part is made or assembled from semi-finished products, such as bar stocks or sheet metal, with well-defined mechanical properties not affected by the shaping process itself or affected in a well-defined fashion (such as in deep drawing, forging, bending, or joining processes). Generally, the design is based on the certified properties of a semi-finished material.

The development of processes for in-space manufacturing is facing additional challenges, as follows.

(1) The physical parameters are very different from those on Earth. In addition to gravitation (from microgravity to the reduced gravity on the Moon and Mars), the atmosphere/vacuum, temperature, and radiation need to be considered.

When manufacturing on Earth, these physical parameters are normally constant, and are thus not considered. Therefore, a new set of variable parameters must be added to the classical "structure-processing-properties-performance" paradigm in materials science and engineering (Fig. 1(a)), to form a new paradigm, i.e., "structure-physical parameters in space-processing-properties-performance" (Fig. 1(b)). In this context, it is important to point out that certainly no "new" physics - different from those in a regular lab environment on Earth - exist in space, but the development of processes for the generation of parts and materials in space remain bound to on-Earth/tellurian conditions, as there are simply not sufficient lab capacities in space.

(2) The properties of the feedstock might be well-defined, but even for industrial processes, the development of feedstock and process needs to be parallelized. Moreover, when it comes to ISRU, the properties of the feedstock are not well-known, and the material availability for studies on Earth is very limited. Simulants are generally used for technology development, such as Moon and Mars regolith simulants, with varying compositions and properties. The challenge is to develop technologies and processes able to accept feedstocks within a certain range of properties.

(3) The availability of platforms for experimental work in space or simulating space environments is generally limited. Parabolic flights provide this opportunity multiple times in a flight for approximately 20–30 s, depending on the level of reduced gravitation to be simulated. On parabolic flights, engineers and scientists have a rare opportunity to convert their experimental setup into a simulated space environment [2]. Sounding rockets are considered as a time- and cost-effective platform for conducting a wide range of experiments under microgravity conditions in space. Using unmanned and suborbital trajectories, these rockets typically offer a few minutes of high-quality microgravity time at altitudes of over 100 km, allowing scientists and engineers on the ground to monitor or remotely control experiments in real time [3]. Orbital microgravity platforms offer long-term microgravity time, the possibility of remote control experiments from the ground, and, depending on the vehicle sample, a return. Space stations additionally offer basic support from crew for scheduled tasks.

In the technology development for ISM, in addition to the duration and quality of the microgravity, the number and frequency of iterations in the manufacturing process are other important parameters. Each iteration includes the preparation and execution of a manufacturing process, retrieval of samples, and analysis of the manufactured object and process data. Data can be transmitted to engineers and scientists on Earth; for the sample object, this takes more time and effort. On this basis, for parabolic flights, an iteration can be performed within a certain number of days during an ongoing campaign. For sounding rockets, the iteration cycle is usually still within months, whereas for orbital platforms and space stations in particular, the iteration cycle can reach years. To overcome this limitation and perform iterations, adaptions, and the like, in that sense, a real development of technology in space would require a team of dedicated space scientists. Currently, such a microgravity platform is not yet available.

To more specifically describe the demand, in the first step, it is necessary to clarify the impacts of each physical parameter on the properties of the material, production process, and technology. For instance, missing gravitation has a limited effect on the material, but has strong implications on the process and technology. In contrast, vacuum often has limited effects on the process and technology, but has a significant effect on the material. A better understanding of these relations, one-by-one, would help in effectively designing experiments and choosing the appropriate platforms.

Generally, the application dictates the type of material and feedstock to be used, depending on the requirements for fulfilling the limitations (Fig. 2). For example, building a habitat on the Moon following the ISRU approach implies the use of lunar regolith dust, which, for the develop-

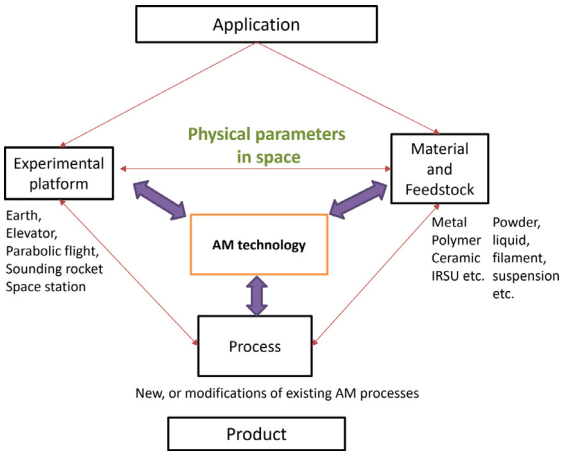

Fig. 2. Inputs and parameters to be considered for the development of technologies for space additive manufacturing (AM).

Table 1
Platforms available for technology development in microgravity, corresponding time available in microgravity and iteration cycle length.

	μg-time	Iteration cycle
Drop tube	Up to 9 s	2 per day
Parabolic flight	21 s	1 per day, 3–4 campaigns per year
Sounding rocket	6.5 min	1 per year
Reentry satellite	Days	Multiple years
Space station	Weeks	Multiple years
Microgravity lab (envisioned)	**Weeks**	**Hours**

ment of the technology, is generally substituted for with a simulant from Earth.

As already mentioned, AM materials and processes are uniquely engaged. Additionally, the influence of the varying physical parameters on the materials and process needs to be considered, as it underlies the entire technology development. These parameters vary because the development of processes remains bound to conditions on Earth, whereas the conditions prevalent in space are generally simulated, and are not available continuously. For example, machinery, materials, and processes might be tested in a vacuum, under an extreme temperature, and/or under reduced gravity or microgravity, but it would be impossible to provide this combination of space-simulating parameters throughout the entire development phase. Thus, the technology must be designed to work not only in space, but also in the usual lab conditions, so that it can be tested and further developed. Therefore, the choice of one or multiple experimental platforms inevitably depends on the application, and imposes certain boundary conditions on the physical parameters that can be tested and their effects on the materials and process. Space stations are quite unique in this context, as they can represent both a final application for AM (such as producing spare parts on board), but also a platform for developing AM technologies in space.

Different strategies are available for simulating the space environment. However, very few of them provide space-like conditions for a long period of time, and with access to the experiment by the scientist. Table 1 illustrates the complexity of the task in developing manufacturing technologies for space AM.

2. Existing Work

AM in space has been proposed for several applications, from the manufacturing of spare parts on the International Space Station (ISS) to the fabrication of satellites and structures in space, to the construction of habitats on the surface of the Moon and Mars.

Technologies for producing parts of all material classes (polymers, metals, and ceramics) are being developed and tested onboard parabolic flights and/or onboard space stations.

A prominent example is the AM Facility (AMF) onboard the ISS since 2016, which is the first commercial AM facility ever installed in space. Since then, hundreds of polymeric parts have been fabricated by a fused deposition modeling 3D printer developed by Made in Space Inc. Currently, the facility is commercially available to governmental and private institutions to produce parts in space. Over the years, the palette of available materials has been expanded to acrylonitrile butadiene styrene, high-density polyethylene (HDPE), and polyetherimide/polycarbonate. In 2020, the first 3D printer for ceramic materials based on Vat photopolymerization technology was installed, further expanding the capabilities of the AMF. A similar technology based on digital light processing was also tested in a parabolic flight by the Chinese Academy of Sciences in 2018, aiming to produce ceramic green bodies.

In October 2019, Made in Space, in partnership with the Brazilian company Braskem, installed a plastic recycling facility for 3D-printed parts. A similar system, called the “Refabricator,” was also installed by NASA and developed by Tethers Unlimited.

The latest development from Made in Space Inc. is the VULCAN system, a platform capable of multi-material manufacturing combining polymer extrusion, metal welding, and computer numerical control machining. NASA is also working on the development of a FabLab, including AM, subtractive manufacturing, and multi-material capabilities.

In 2019, Techshot Inc., a partner of the ISS National Laboratory, together with nScrypt, developed the 3D BioFabrication Facility (BFF). The BFF uses human cells (such as stem or pluripotent cells) and tissue-derived proteins as bio-inks for 3D printing.

In parallel, Tethers Unlimited, contracted by NASA, is developing capabilities for the in-space manufacturing and in-space assembly of large-scale truss structures, antennas, and satellites.

In the past few years, AM in space has attracted much attention, as it is considered a key technology for the development of a low-Earth commercial space economy [4]. In 2020, the ISS U.S. National Laboratory also organized a workshop dedicated to AM in space. The ISRU approach can further expand the capabilities of AM in space, especially to support future plans for exploration and colonization of the Moon and Mars.

Many AM methods have been proposed and tested with lunar and Martian simulants for different envisioned scenarios, from the manufacturing of small components to the construction of the European Space Agency’s (ESA) envisioned Moon village [5]. A recent overview can be found in a book chapter by Goulas et al. [6].

The nature of regolith facilitates approaches in which the feedstock is used directly as a powder or suspension. Extrusion processes have been proposed for applications at different scales, and with different feedstocks. Extrusion-based AM for small ceramic (from a colloidal suspension [7], or polymer-ceramic [8]) components has been tested with Martian and lunar simulants. Contour crafting, a technology following the principle of extruding a cementitious paste, has been applied to large-scale structures with sulfur-based concrete. An alternative technology developed by D-Shape and tested for ESA with the lunar simulant DNA-1 is based on powder bed 3D printing [9]. This technology works by depositing powder layers and selectively jetting a liquid, thereby inducing a setting reaction in the material. A major disadvantage of this approach and of extrusion technologies in general is that they rely on a liquid phase that either needs to be carried from Earth or synthesized in space.

In contrast, laser-based technologies rely only on the use of regoliths and energy sources. However, controlling the sintering and melting of the regolith is challenging, as both lunar and Martian regoliths have complex chemical and mineralogical compositions influencing their melting behaviors [10]. Most of the current research is dedicated to laser powder bed fusion AM processes, as proposed by Balla et al. [11] and Fateri et al. [12].

An interesting alternative to the use of lasers for powder bed fusion is the use of solar concentrators [13], which has the advantage of using both a feedstock and an energy source readily available on the surface of the Moon.

Owing to the complexity of ISRU materials, there are very few studies in which the processes have been tested in simulated lunar or Martian conditions. The atmosphere has a strong influence on the behavior of a material, especially during sintering and melting; therefore, it is essential that processes are tested under conditions similar to those on the lunar surface (almost no atmosphere) or on the Mars surface (low atmospheric pressure of 6–7 mbar (1 mbar=100 Pa), with a 95% CO_2 composition).

Adding to this challenge, access to platforms on which both gravitation (lunar/Martian) and atmosphere can be simulated is very restricted. A recent study in this direction was described by Reitz et al. They tested the laser melting of a regolith simulant developed and manufactured at TU Braunschweig in vacuum conditions in the Einstein-elevator, and compared the results at 0*g* (no gravity), 0.16*g* (lunar gravity), and 1*g* [14].

Section 3 presents some of the first results from laser powder bed fusion studies of different combinations of feedstocks, atmospheres, and experimental platforms: (i) steel and regolith simulants in a nitrogen atmosphere and vacuum, and at microgravity, lunar, and Martian gravitational acceleration, as tested onboard a parabolic flight; (ii) laser powder bed fusion of a metallic glass on a sounding rocket, and (iii) AM with long fiber-reinforced polymers in space.

3. Strategies for Space AM Technology Development

In this chapter, examples of the development of space AM technologies are presented, with a focus on different applications.

3.1. Laser beam melting (LBM) of metal and regolith simulants on parabolic flights

3.1.1. Parabolic flight campaigns

The working principle of gas-flow-assisted powder deposition was tested under microgravity conditions and continuously improved over the course of the 30th, 31st, 33rd, 34th, 36th (in combination with the Deutsches Zentrum für Luft- und Raumfahrt (DLR), and the 76th ESA campaigns of parabolic flights, as operated by the French company Novespace in Bordeaux.

During the campaign, the experimental setup was mounted onboard an appositely modified Airbus A310. The airplane flew a parabola consisting of three phases. In the first phase, the airplane gradually reached an inclination of up to 47°. In this phase, named “pull-up,” an increased acceleration of 1.8*g* (hypergravity) acted in the direction perpendicular to the floor of the airplane. After reaching 47° nose up and flying the cap of the parabola until 42° nose down, 22 s of microgravity were experienced. This was followed again by 1.8*g* of “pull-out” at the end of the parabola, transferring the steep descent into a horizontally oriented steady flight phase.

Each campaign consisted of three to four flights with 31 parabolas consecutively flown in one flight, summing up to approximately 34–45 min of microgravity.

As with commercial laser beam melting (LBM) equipment, gas-flow-assisted powder deposition parts are manufactured layer-by-layer. Each layer consists of two steps: 1) deposition of a thin powder layer, and 2) inscribing/”printing” the respective layer information by selectively laser-melting the powder.

During the campaign, one layer (100 μm thick) was deposited in the microgravity phase of each of the 31 parabolas, resulting in a maximum height of 3.1 mm of the parts manufactured in one experiment. As the 22 s at microgravity was not sufficient to complete both process steps, the layer deposition and laser melting had to be performed in different stages of the parabolic flight.

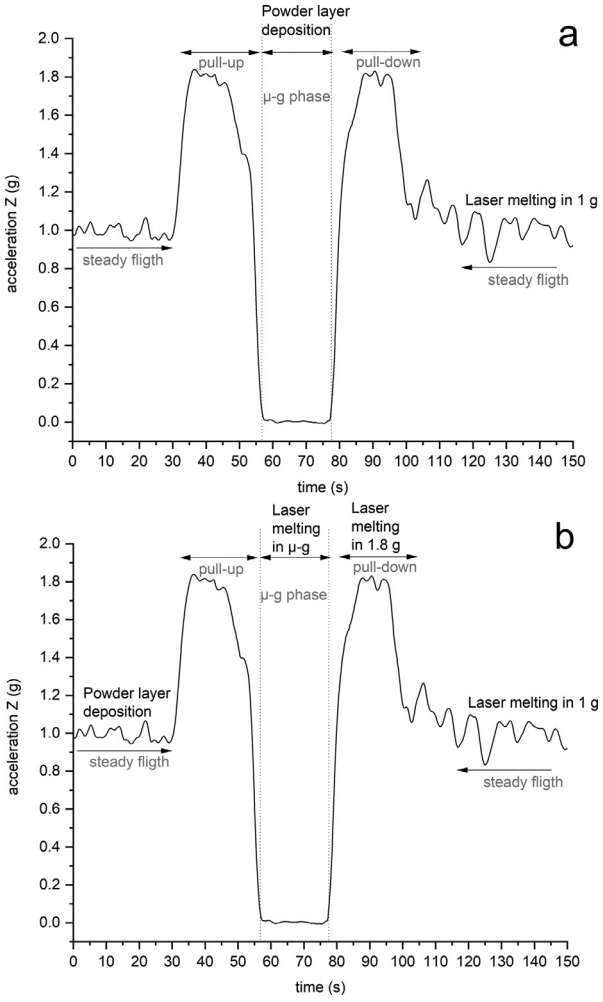

Fig. 3. (a) Experiment configuration a to test the powder deposition in microgravity conditions; (b) Experimental configuration b to test the laser melting in microgravity, 1*g*, and 1.8*g* conditions.

The primary objective of this work was the development and continuous improvement of the deposition of powder layers under microgravity by the gas-flow assisted powder deposition process following experiment configuration (Fig. 3(a)), which was performed in the 22 s microgravity phase, followed by laser melting in the successive steady flight phase.

In addition, the effects of different acceleration conditions in the laser melting step were studied. For these studies, experiment configuration as shown in Fig. 3(b) was chosen. The powder deposition was performed in the 1*g* steady flight phase before the parabola. Successively, one set of samples was laser-melted in the microgravity phase, followed (in the same layer) by one set of samples laser-melted in the 1.8*g* hyper-gravity phase, and finally, by one set at 1*g*.

The custom setup built for the experiments consisted of two racks, as shown in Fig. 4.

The powder deposition unit and laser system, which included the laser module, scanner, and optics, were mounted on rack 1. This unit included an actual LBM system. The building platform, 106.5 mm × 85.5 mm in size, was made of a 5 mm thick sinter metal plate (stainless steel AISI 316L/B) with a grade efficiency of 9 μm.

A gas circulation pump used for evacuating and purging the system with nitrogen, electrical cabinet, and computers to control all operations of the LBM system (that is, the layer deposition and laser) were mounted on rack 2.

Fig. 4. Photo of the two racks setup for laser beam melting (LBM) at microgravity as mounted in the airplane (Rack 1 (right) includes the LBM system, rack 2 (left) vacuum includes the pump and computers to control the process).

3.1.2. Process idea for LBM at microgravity

In LBM, a flowable powder is spread layer-by-layer, and the layer information of the part is printed after each consecutive layer deposition step. Generally, layer deposition requires gravitational forces acting on each particle as a prerequisite for the compaction of the particles and the formation of a smooth layer. To compensate for the missing or reduced gravitational forces in space or on the Moon, the "gas flow-assisted powder deposition" has been developed. An additional force acting on each particle is introduced by establishing a gas flow through the powder bed. The gas-flow-assisted powder deposition is based on a porous building platform acting as a filter for the fixation of the particles in the gas flow, and is driven by a reduced pressure established by a vacuum pump underneath the platform. In combination with a laser source and scanner, this technology can provide ready-to-use metal or polymeric parts manufactured in space.

To test and further develop this technology, an experimental machine qualified for DLR and ESA zero-*g* parabolic flight campaigns was developed, and was included in five parabolic flight campaigns. A schematic of the setup is shown in Fig. 5.

The gas flow established by means of the vacuum pump throughout the powder bed imposes a drag force on the particles, which on average is directed towards the porous building platform, that is, in the direction in which the gravitational force would normally act, as shown in Fig. 6. Where F_{pp} representing the interparticle force, and F_d the force induced by the flow field of the gaseous medium throughout the powder bed and porous support.

This force can stabilize the powder bed even when the gravitational force is absent. The porous building platform not only supports the powder, but also acts as a filter to prevent the powder from being dragged into the pump. The vacuum pump is attached via a conventional vacuum hose and vacuum-tight adaptor plate to the porous base plate. The powder delivery systems, the so-called recoater, are roller-type with a separate gas-flow-stabilized reservoir, or box-type.

3.1.3. Simulated scenarios of LBM at reduced gravitation on parabolic flights

The equipment described in Section 3.1 was used for the deposition of metal powders and lunar regolith simulant (EAC-1A type) in the course of four DLR parabolic flight campaigns and of the 76th ESA campaign. This campaign offered a combination of microgravity and Moon and Mars gravitations in each of the three flight days, alternating in five consecutive parabolas at one acceleration. With 30 parabolas on one flight day, 10 parabolas of one acceleration were available in one flight.

Fig. 7 provides an overview of the experiments that could be performed with the variable physical parameters, e.g., atmospheric pres-

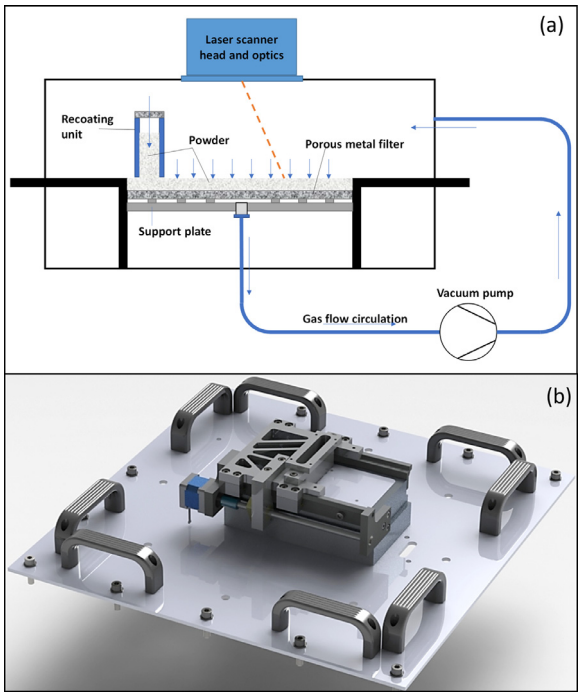

Fig. 5. (a) Schematic of the gas flow-assisted powder deposition; (b) Rendering of the powder deposition unit (the area of porous building platform for the powder deposition was 106.5 mm × 85.5 mm).

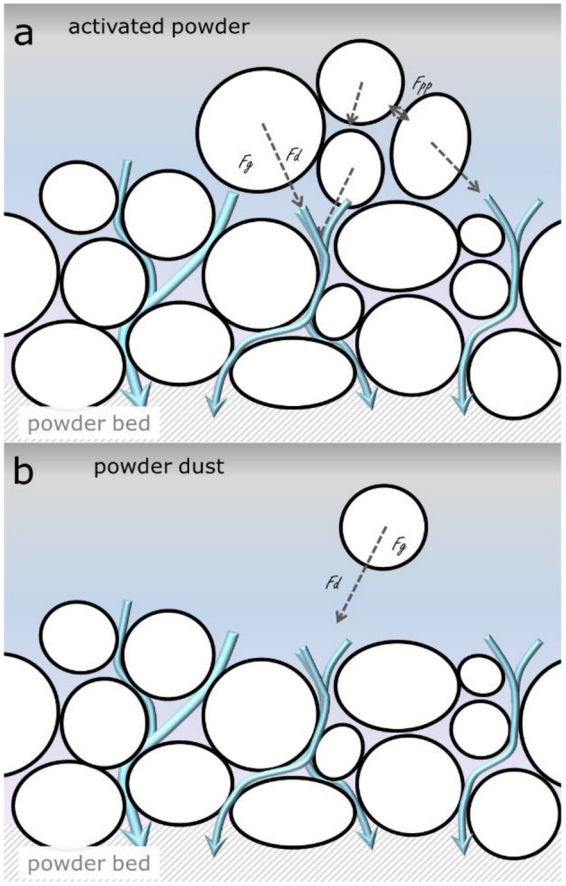

Fig. 6. Illustration of the forces acting on each individual particle during layer deposition in the gas flow-assisted powder deposition: (a) deposition of a flowable but compact powder, and (b) deposition of a dust.

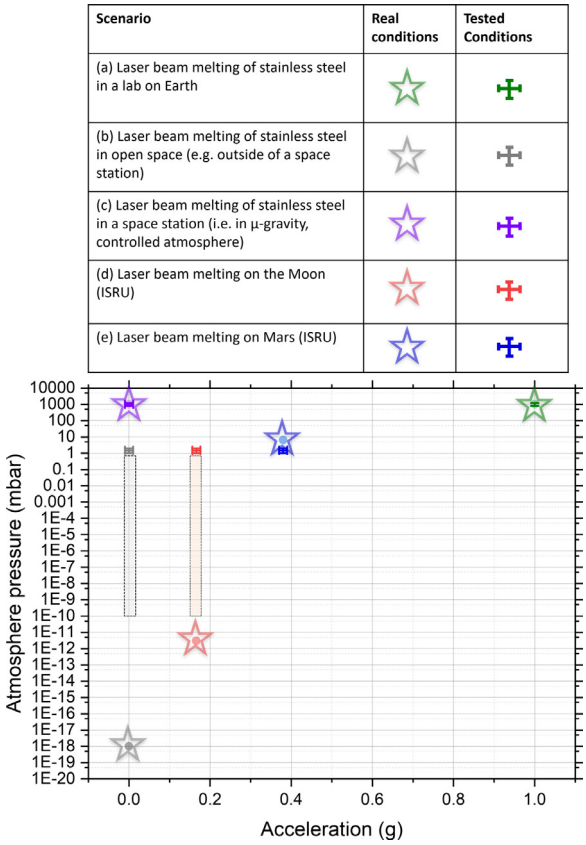

Fig. 7. Matrix of experiments following the physical parameters of gravitation (acceleration) and atmospheric pressure.

sure and gravitation (acceleration). Additionally, different scenarios could be mimicked and evaluated, as shown in the graph.

In the following, the scenarios listed in Fig. 7 are introduced briefly, and the corresponding results are highlighted.

- **LBM of Stainless Steel in a Laboratory on Earth**

Description of scenario: The LBM of metals on Earth represents the reference point for experiments under different gravitation and atmospheric conditions. LBM is a well-industrialized and widely studied process, therefore details of the investigations are not given here. In this context, it should be noted that LBM processes are generally conducted in a protective atmosphere (close to ambient pressure) with a gas flow of argon or nitrogen. In contrast, electron beam melting is generally performed under vacuum. In this study, the LBM of stainless steel in a nitrogen atmosphere was used as a reference.

The optimization of an LBM process is a complex task, with various parameters to be optimized. Because it is unrealistic to perform this optimization during a parabolic flight, most parameters need to be tested and set in the laboratory. In this sense, a full process development in controlled acceleration conditions is not feasible, and for most parameters (e.g., laser power and scanning speed), only small adjustments starting from pre-set laboratory values are possible.

- **LBM of Stainless Steel in Open Space**

Description of scenario: With a given metal powder and a laser system, it is possible to fuse metal particles in a low-pressure (vacuum) atmosphere. At pressures lower than 10^{-8} Pa, the reaction of the metal powders with the atmosphere is virtually non-existent. The powder layer deposition process in principle could be performed in open space e.g. by means of a rotating drum and feeder system to simulate gravitation. However, such a system has not been built or tested (for now).

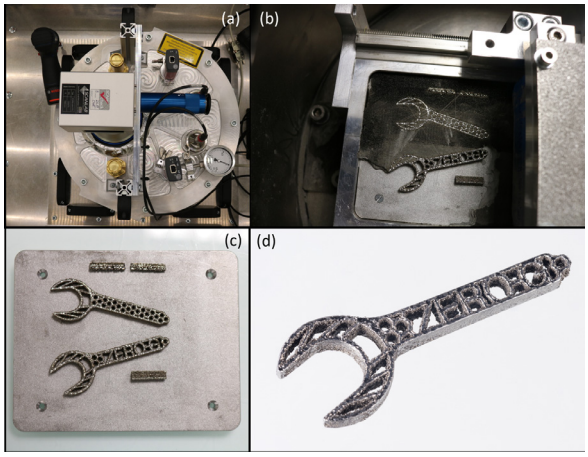

Fig. 8. (a) Top view of the deposition chamber, showing the laser scanner and optics, two oxygen sensors, two pressure gauges, and two overpressure safety valves; (b) View of the deposition unit during cleaning after a parabolic flight, showing the wrenches produced by LBM still partially embedded in the powder bed; (c) Top view of the porous metal base plate on which the wrenches were manufactured in microgravity; (d) 12 mm wrench manufactured in microgravity, after separation from the base plate (the base plate has a size of 106.5 mm × 85.5 mm).

- **LBM of Stainless Steel at Reduced Gravity, in a Controlled Atmosphere**

Description of scenario 1: To manufacture spare parts and other components on-demand on board a space station or spacecraft, powder-based LBM is one option. From a technological perspective, the equipment used could resemble those for industrial use on Earth, but it would need to compensate for the missing gravitation in the layer deposition process of the powder.

Experimental setup: The LBM setup introduced in Section 3.1.2 was used for the listed experiments. For the related experiments, the atmospheric pressure in the process chamber, as purged and backfilled with nitrogen, could be adjusted to approximately 850–950 mbar. The gas flow was adjusted in the range of 15–30 l_n/min. A detailed discussion of the effect of gas flow is given in Ref. [15]. The laser melting was performed at a laser power output of approximately 120 W of continuous wave.

Results: In Section 3.1.2, the related technology was introduced. A 12-mm wrench was chosen as a proof-of-concept for the LBM process in microgravity. The wrench had a handle with a length of approximately 55 mm and a lightweight design. Fig. 8(a) shows a top view of the LBM process chamber containing the powder deposition unit. The laser scanner and collimator, three pressure gauges, and two overpressure valves were mounted on the top of the chamber.

Fig. 8(b) shows the powder bed after partial removal of the powder, as deposited in microgravity during 31 parabolas and with the two laser-melted wrenches embedded. The same samples are shown on the porous metal plate (Fig. 8(c)) after cleaning. The "ZERO-G" wrench is shown in Fig. 8(d) after its separation from the base plate.

These samples are the first metal parts ever 3D-printed in microgravity by LBM. The building strategy corresponds to experiment configuration illustrated in Fig. 3(a), that is, layer deposition in microgravity followed by laser melting during steady flight at normal gravity.

From a qualitative point of view, no major differences are observed between parts laser melted in 1*g* and in microgravity conditions, as described in a previous work in Ref. [15]. Nevertheless, owing to time limitations, it is not possible to test both powder deposition and laser melting in the microgravity phase of the same parabola in a parabolic flight. For a detailed study of the influence of microgravity on the LBM material, sounding rockets are a more suitable platform, as they provide high-quality microgravity conditions for a longer period of time.

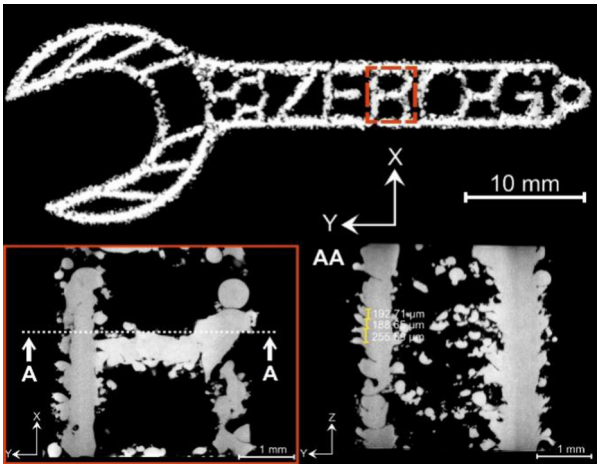

Fig. 9. Computed micro-tomography reconstruction of a wrench produced at different accelerations: moon, microgravity, Mars.

Description of scenario 2: Metallic materials will play an essential role in installing a permanent human base on the Moon. In this context, AM offers, arguably even more than on Earth, the possibility of the flexible production of small-to medium-sized metallic parts. Moreover, the manufacture of spare parts and components from metals and polymers is an important factor for increasing the resilience of missions.
Experimental setup: The LBM setup introduced in Section 3.1.2 was used for the listed experiments.
Results: The same "ZERO-G" wrench shown in Fig. 8 (manufactured in microgravity) was produced by LBM in a mixed parabolic flight with 10 parabolas in microgravity, 10 at simulated Moon gravitation, and 10 at Mars gravitation.

This sample was imaged by X-ray micro-computed tomography (μCT) using a commercial ZEISS Xradia 620 Versa μCT machine. Two imaging approaches were used to obtain an overview scan and a more detailed one. First, an acceleration voltage of 150 kV and power of 23 W were used. The X-ray spectrum was filtered on the source side using a device-specific filter named HE18. A geometrical magnification of approximately 2.7× with a source-to-object distance of 130 mm and object to flat-panel detector of 230 mm was reached. This yielded an effective pixel size of 27 μm. The detailed scan used an acceleration voltage of 160 kV and power of 25 W. The X-ray spectrum was filtered using an HE5 filter. The distance between the source and the object was set at 30 mm and that from the object to the detector was set at 20 mm, giving a 1.6× geometrical magnification. With the help of an optical magnification of 4×, an effective resolution of 4 μm was achieved. 3D tomographic datasets with 1601 and 3201 angular object projections were reconstructed, respectively, using the automated reconstruction routine from the machine. The processing of the reconstructed data was conducted using non-commercial licensed software Dragonfly (Object Research Systems, Canada).

Fig. 9 can be distinguished into three images, i.e., the top, bottom-left, and bottom-right image. The top image shows the result from the first imaging approach with the image resolution of 27 μm. It is evident that in principle, the structure of the wrench can be printed under reduced gravity. The images on the bottom part are the result from the second imaging approach with the resolution of 4 μm. The red box on the top image indicates the region where the second imaging approach was conducted. Thus, the higher resolution image of the exact slice can be seen on the bottom-left image. A section line (depicted by the white dashed line) shows the origin of the bottom-right image that indicates the corresponding cross-section.

- **LBM of Regolith (ISRU) and Steel on the Moon and Mars, Performed in the 76th ESA Flight Campaign.**

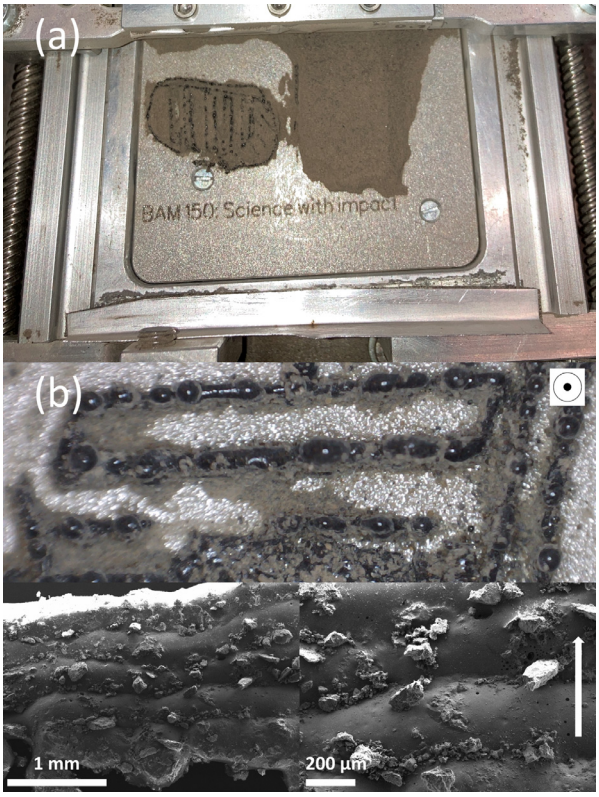

Fig. 10. (a) Laser sintered regolith samples, still attached to the base plate of the LBM machine: sample produced during a parabolic flight at Moon and Mars acceleration (0.16*g* and 0.38*g*, respectively); (b) Enlarged optical image of the sample, showing typical balling defects (The lower part shows two scanning electron microscope (SEM) images of the same sample. The circle and arrow indicate the direction of stacking of the layers, respectively).

Description of scenario: To build habitats on the Moon and Mars, the use of local resources is crucial. The materials available need to be researched; moreover, processes for manufacturing parts and building infrastructure need to be envisioned, developed, and tested.
Experimental setup: The LBM setup introduced in Section 3.1.2 was used. For the related experiments, the process chamber was evacuated to a minimum pressure of approximately 110 Pa. This pressure was still higher than the lunar atmospheric pressure, but it was within the range of the Martian atmospheric pressure, which could be simulated. At 100 Pa, the mean free path of air or nitrogen molecules is approximately 60 μm; thus, it was in the range of the particle size of the regolith particles used. As mentioned in the previous section, a scroll-type vacuum pump providing the gas circulation, in this case, was employed for the evacuation of the system. A better vacuum can be achieved by using an additional vacuum pump. However, the level of the vacuum on the surface of the Moon (approximately 3×10^{-12} mbar at night) is achievable only in ultra-high vacuum chambers on Earth, and cannot be realistically obtained in a chamber containing equipment and powders for LBM.

The laser melting was performed at a laser power output of approximately 20 W for the regolith.
Results: Fig. 10 shows EAC-1A lunar simulant laser sintered onboard the airplane during a parabolic flight at the Moon and Mars accelerations (0.16*g* and 0.38*g*, respectively).

It can be seen that the quality of the part and homogeneity of the material are considerably decreased at reduced gravitational acceleration relative to similar experiments performed in a normal laboratory environment. Only at some points can a good joining between layers be achieved.

Table 2
Matrix of experiments following the physical parameters gravitation (acceleration) and atmospheric pressure performed in the 76th ESA parabolic flight campaign at simulated Moon and Mars gravitation.

Atmosphere	Acceleration Lunar-gravity	Martian-gravity
Vacuum/ minimum pressure	(I) ISRU on Moon surface. Material: EAC-1A	(II) Simulating ISRU via LBM on martian surface. Material: EAC-1A
> 100 Pa	(III) AM of 316L directly at lunar atmosphere	
N_2 atmosphere	(IV) Simulating AM via LBM at varying accelerations in space with gas flow assisted powder deposition. Material: EAC-1A and steel 316L	

Most likely, this is related to the fact that the packing density of the powder layers as deposited on the simulated Moon and Mars gravitation is drastically lower than that of normal gravitation. In contrast to previous experiments with metal powder, performing the experiments in a vacuum does not allow for the application of a gas flow through the powder bed. This greatly reduces the packing of the powder during the deposition of layers at reduced gravitation.

In addition, a typical balling effect, with the formation of spheres of the molten material, is also visible in Fig. 10. Balling is a well-known type of defect that can arise during LBM, and is caused by a lack of wetting between the molten material and the cold material of the previous layers or substrate. As in this case, balling is considerably worsened when the packing density of the powder bed is low, as observed in the samples produced at Moon and Mars gravitational accelerations. This result highlights the challenges in transferring process design parameters from a laboratory on Earth to a platform at reduced gravitational acceleration.

3.1.4. Summary of the Results

Table 2 provides an overview of the experiments performed in the 76th ESA parabolic flight campaign, combining different accelerations, atmospheric conditions, and materials.

3.2. LBM on sounding rocket mission

Since its maiden flight in 2009, the MAPHEUS sounding rocket has been launched on an annual basis by the DLR. The rockets are launched from the ESRANGE Space Center [16] near Kiruna, Sweden, which is run by the Swedish Space Corporation. MAPHEUS is dedicated to microgravity research, mainly for materials science and technological development. Experimental hardware from various fields of materials physics have been aboard MAPHEUS rockets, and flight hardware has been developed and qualified in-house by the Institute for Materials Physics in Space, as accompanied by ground reference experiments [17–22]. This allows for rapid development cycles and a reduction in lead time, so as to advance scientific objectives. The scientific payloads consist of several experimental facilities, and sum up to 300 kg.

The vehicle uses a two-stage configuration of solid propellant rocket engines, carrying a scientific payload, control and communication systems, a recovery system, and a rate control system. The total length is approximately 12 m with a 17 in (438 mm) payload diameter and lift-off mass of 2.7 t [26, 23, 24], as shown in Fig.11.

After lift-off, the vehicle performs a hypersonic suborbital flight following a ballistic trajectory. After burnout of the second stage and at an altitude of 90 km, a three-axis rate control system is engaged to actively control the rotational rate towards zero using cold gas thrusters, thereby establishing a microgravity level below $10 \times 10^{-4} g$ on board. The remaining acceleration level is mostly owing to drag in the high atmosphere and reduces to $10 \times 10^{-6} g$ near the apogee at 250 km, where the vertical velocity decreases to zero. During descent, the microgravity time ends at 90 km when the payload prepares for reentry into the denser atmosphere. The total microgravity time above 90 km is 325 s. After deceleration to subsonic speed by atmospheric drag, a two-stage parachute system is activated, and the payload touches the ground in the designated landing area. It is then recovered by helicopter and brought back to the laboratory for further investigation, usually within hours.

Fig. 11. MAPHEUS-11 vehicle during test countdown. Two-stage solid propellant engine (orange), and several experiment units (golden) stacked on top. The vehicle has a total length of approximately 12 m and carries 300 kg of scientific payload to an apogee of 250 km, allowing over 6 min of microgravity.

During flight preparation prior to lift-off and throughout the flight, there is telemetry and telecommand communication to the ground station and TV channels. Engineers and scientists are therefore able to supervise ongoing experiments in real time and manipulate the programmed automatic sequence if necessary.

One experimental facility designed for performing AM on a sounding rocket is the “Multi-Material Additive Manufacturing for Research and Spaceflight” (MARS) system, as shown in Fig. 12. It is a state-of-the-art setup specially designed for the MAPHEUS sounding rocket, and is able to perform an LBM manufacturing process in microgravity by employing the previously described gas-flow-assisted powder deposition developed by the Bundesanstalt für Materialforschung und -prüfung. The overall dimensions measure only Ø390 mm × 700 mm at 56 kg.

MARS is a compact and lightweight yet fully automated functioning and autarkic device available to investigate and further develop LBM technology in weightlessness, under Moon, Mars, or Earth gravitation, and is designed and tested to withstand up to 25*g*. MARS has been run through functional and environmental testing, and has gained flight qualification for space flights aboard the MAPHEUS sounding rocket. It was used for the first time in microgravity during the DLR parabolic flight campaign in 2019, with a focus on system testing and calibration of the powder handling and layer application.

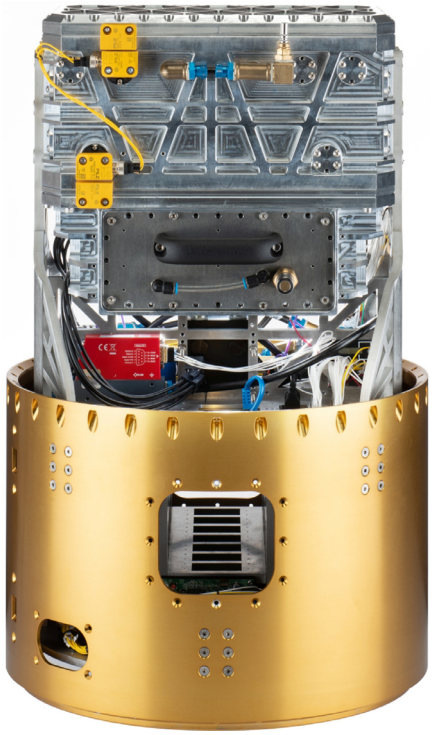

Fig. 12. "Multi-Material Additive Manufacturing for Research and Spaceflight" (MARS) set-up for laser beam melting of parts from metal powders in space.

In 2021, MARS performed its first space flight on MAPHEUS-11, and succeeded in additively manufacturing a metallic part in space. Investigations on flight samples are still ongoing, the results of which will be published later. The advantage of the MAPHEUS sounding rocket over parabolic flights is that there are no hypergravity phases between the powder layer deposition and laser melting phases. This allows the experiment to run under a larger combination of space-simulating parameters, which, as previously mentioned, is invaluable in the development of in-space AM technologies. As a matter of fact, it is known that the lack of gravity or reduced gravity affects the crystallization of a melt [25, 26]. This highlights the importance of metal-based AM experiments on sounding rockets, at least until microgravity labs are more readily available. Additionally, the powder used in this first space flight was a zirconia-based bulk metallic glass, making this experiment a world premiere. LBM has recently been shown to circumvent the usual size limitations in the manufacturing of bulk metallic glasses [27–29]. Indeed, instead of having to cast the whole part, it can be produced layer-by-layer, and still retains its glassy structure, thereby providing bulk metallic glasses with much more flexibility in terms of design and manufacturing.

3.3. Fiber-reinforced polymers

3.3.1. 3D printing of advanced special plastics in extreme environment

A 3D printing system with a controllable ambient temperature was developed to investigate the influences of the ambient temperature on the crystallinity and tensile strength of polyether ether ketone (PEEK) samples prepared by material extrusion, as shown in Fig. 13.

When the ambient temperature was increased from 25 °C to 200 °C, the crystallinity of the 3D-printed PEEK samples increased from 17% to 31%, significantly reducing the breakage elongation of the samples to less than 20%. Meanwhile, the tensile strength and modulus of the PEEK samples were also increased from less than 60 MPa to 80 MPa, with improved crystallinity. For space applications, the structural stiffness, temperature, and UV radiation resistance of 3D-printed components are

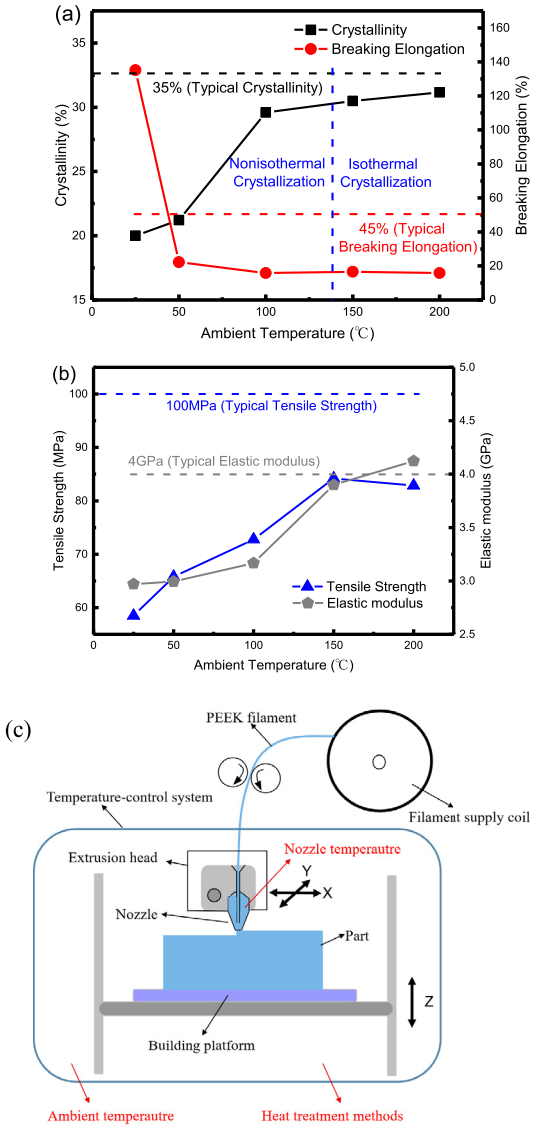

Fig. 13. Influence of ambient temperature on (a) crystallinity and (b) tensile strength [30]; (c) temperature-control 3D-printing system for high-performance polymers.

earlier considerations, and are closely related to the crystallinity of 3D-printed PEEK materials. Thus, an advanced thermal control system for the 3D printing device is critical for the fabrication of stable and qualified PEEK components, owing to the extreme temperature fluctuations in outer space.

However, with the available thermal control technology, a high ambient temperature of 200 °C cannot be maintained stably in outer space, owing to the aforementioned extreme temperature fluctuations and high energy consumption. A new strategy for the 3D printing of PEEK should be conceived by considering another important environmental factor, vacuum.

When an ultra-large structure is planned to be fabricated by in-situ 3D printing in outer space, a vacuum environment is another important factor, potentially with a significant influence on the heat transfer process during 3D printing.

To explore the influence of the ambient pressure on the 3D printing process and performance of the printed components, a 3D printing machine was installed in an environmental testing chamber, as shown in Fig. 14. PEEK samples and components were printed in the chamber with normal and low pressure, respectively, so as to investigate the in-

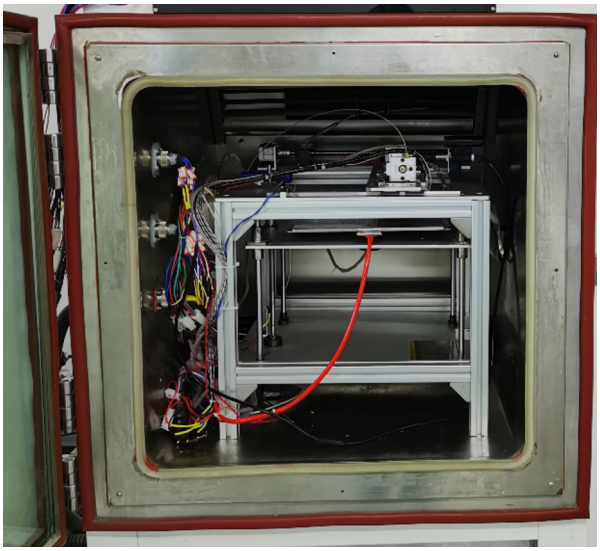

Fig. 14. 3D-printing machine installed into an environmental testing chamber.

fluence of ambient pressure on the 3D printing process and properties of 3D-printed parts. The 3D printing was started from room temperature in the chamber without any thermal control on the ambient environment, which was relatively stable at approximately 30 ˚C during the entire printing process.

As shown in Fig. 15(a), the tensile strength of the 3D-printed PEEK samples evidently increased from 64.0±4.5 MPa to 82.3±1.5 MPa when a low ambient pressure of 100 Pa was applied in the chamber. Differential scanning calorimetry (DSC) analyses were conducted on the PEEK samples prepared using different 3D printing strategies, as shown in Fig. 15(b). For PEEK samples prepared at normal pressure, there is a cold crystallization process at approximately 170 ˚C, which cannot be observed for PEEK samples printed at low pressure. The degree of crystallinity of PEEK materials can also be calculated according to the DSC results, which show very large differences of 14% and 27% for samples printed at normal and low pressure, respectively.

As shown in Fig. 13(a), when the ambient temperature is lower than the initial crystallization temperature of 140 ˚C, the 3D-printed PEEK materials normally have a non-isothermal crystallization character with a relatively low crystallinity, owing to the quick cooling process by thermal convection. However, in vacuum or low-pressure environments, the thermal convection is significantly reduced, and the thermal radiation dominates the heat transfer process. Thus, with the low efficiency of the thermal radiation, heat cannot be efficiently dissipated from the extruded materials. As such, they may reach at a higher temperature than the initial crystallization temperature of 140 ˚C and obtain a high crystallinity and interlayer bonding, as shown in Fig. 16. Meanwhile, owing to the relatively stable temperature field caused by the inefficient heat transfer, the temperature gradient in the 3D-printed part can be reduced, which can decrease its deformation.

Thus, by using low-pressure or vacuum conditions in outer space, a new 3D printing strategy for PEEK and PEEK composites can be realized by normal thermal control (approximately 30 ˚C) and vacuum printing, which can simplify the 3D printing device and reduce the energy consumption required to meet the requirements for space equipment and applications.

3.3.2. 3D-printing and recycling of carbon fiber-reinforced composites

Fiber reinforcement has been widely used to meet critical requirements for space structures, especially in the form of carbon fiber (CF)-reinforced composites. A CF/PEEK composite is a verified material series for typical space applications, owing to its high structural stiffness and temperature resistance. However, all of the CF/PEEK composite components are fabricated on earth using conventional processes, such as fiber placement and injection molding, and then are delivered by rocket. Conventional mold-based forming processes for CF/PEEK composites are not suitable for the in-situ fabrication of large truss structures in space. Thus, new forming processes should be explored and adopted for space manufacturing.

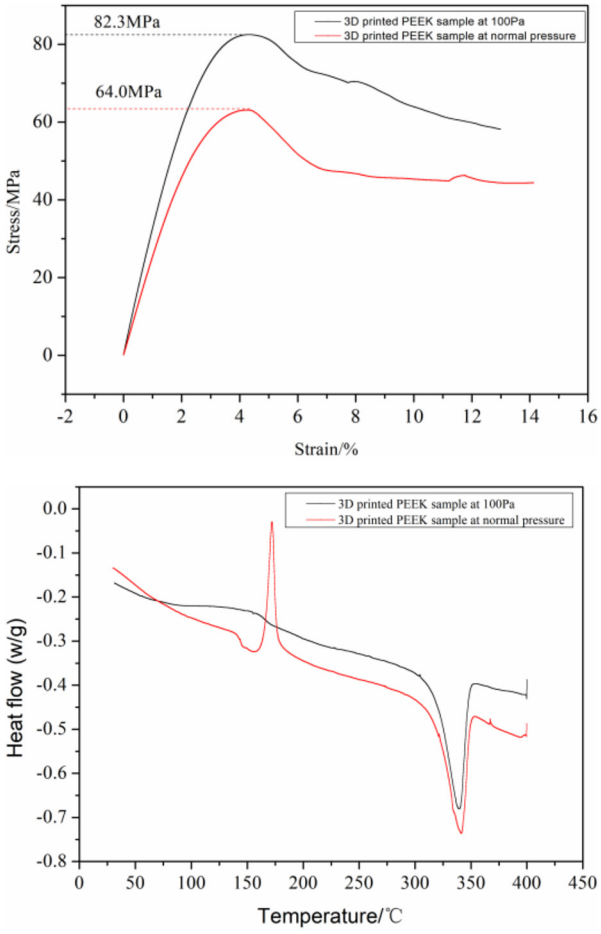

Fig. 15. Tensile strength and differential scanning calorimetry (DSC) analysis results of 3D-printed polyether ether ketone (PEEK) samples at different pressures.

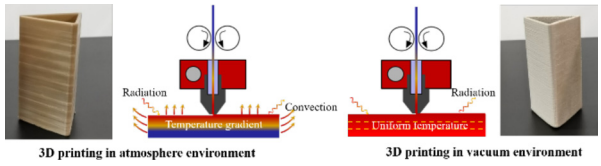

Fig. 16. Different heat transfer procedures in 3D printing processes at normal and vacuum environments.

Recently, the 3D printing of continuous fiber reinforced thermoplastic composites (CFRTPCs) has been developed to realize the rapid fabrication of complicated composite structures by using carbon fiber and plastic filament as raw materials [31], as shown in Fig. 17. The simple formation mechanism, low energy consumption, and compact and compatible raw materials make this 3D printing process very suitable for in-situ fabrication in outer space.

A wide variety of material types have been used in the 3D printing of CFRTPCs, such as carbon fiber, Kevlar fiber, glass fiber as the reinforced phase, and polylactic acid (PLA), nylon plastic, and PEEK as the matrix. The fiber and plastic filament are fed into the nozzle simultaneously and

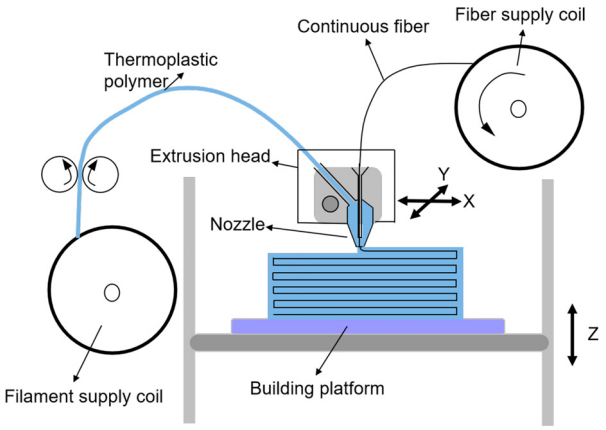

Fig. 17. Schematic of continuous fiber-reinforced composite 3D-printing and some 3D-printed composite components.

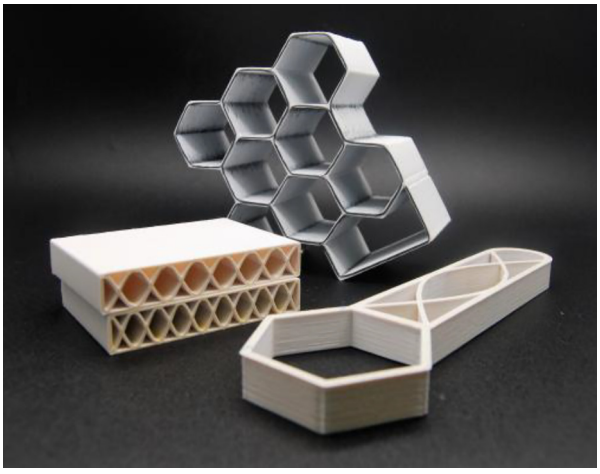

Fig. 17. Continued

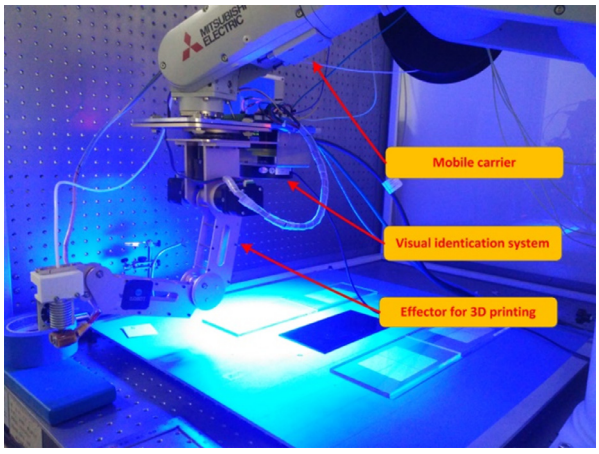

Fig. 18. 3D-printing end-effector on a multi-degree-of-freedom robotic arm.

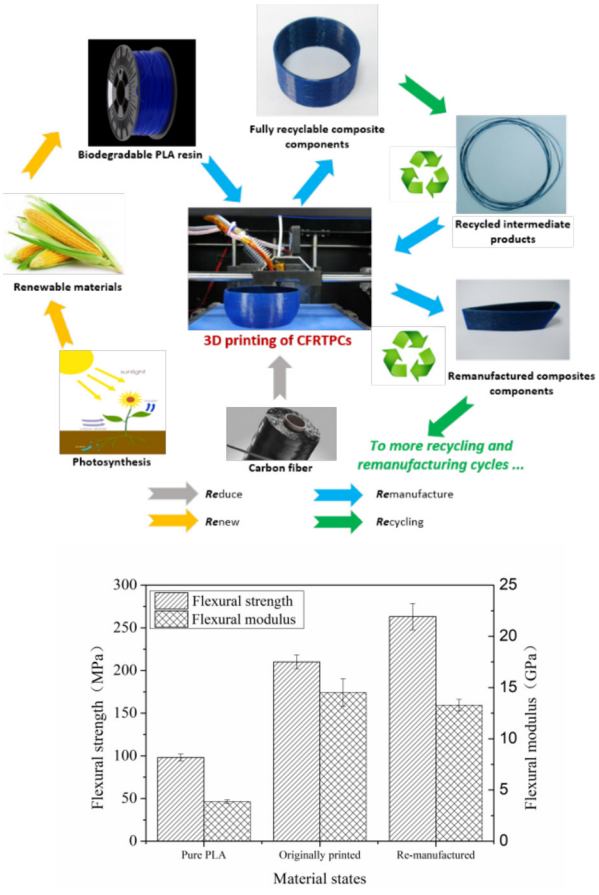

Fig. 19. Recycling and remanufacturing of 3D-printed continuous carbon fiber reinforced polylactic acid (PLA) composites [32].

then impregnated in a liquefier, before being extruded through an orifice onto the platform layer-by-layer. By controlling process parameters such as the hatch spacing, printing speed, printing path, the multiple material interfaces and mechanical performance can be optimized. In addition, the composite preparation and forming are fully integrated into one printing process. Complicated composite components with curvilinear fiber orientations and advanced structural performances can be fabricated. In one example, the tensile strength and modulus of the printed composite samples were 760 MPa and 79 GPa, respectively, i.e., higher than those of aluminum alloys.

A 3D printing process with additional degrees of freedom has also been developed for CFRTPCs with the goal of realizing fiber printing on 3D structures or curved surfaces, as shown in Fig. 18. A curvilinear fiber trajectory could be designed and achieved by careful control of the printing head movement, while making use of the inherent anisotropic properties of the CFRTPC to optimize the overall performance of the 3D-printed structure. This robotic system has also demonstrated the possibility of 3D printing in space with a printing head as an end-effector, and a visual identification system for positioning.

Based on the deposited fiber bundles in the 3D printing composite structure, a recycling and remanufacturing method has been found for realizing an in-situ resource utilization strategy, as shown in Fig. 19. The 3D-printed composites were recycled by locally heating the thermoplastic matrix and mechanically pulling the fibers. The continuous carbon fibers were 100% recycled without significant breakage after thermal recycling in the form of an impregnated carbon fiber filament, which was reused in a secondary 3D-printing process. The remanufactured CFRTPC specimens also exhibited a 25% higher bending strength than the original specimens, which experimentally demonstrated the first non-downgrade recycling process for CFRTPCs. Energy consumptions of 67.7 MJ/kg and 66 MJ/kg were measured for the recycling and remanufacturing processes, respectively, and could be further reduced with an improved design of the local heating device. The combination of 3D printing and recycling for CFRTPCs provides fully recyclable materials and a formation strategy for future composite structures in space.

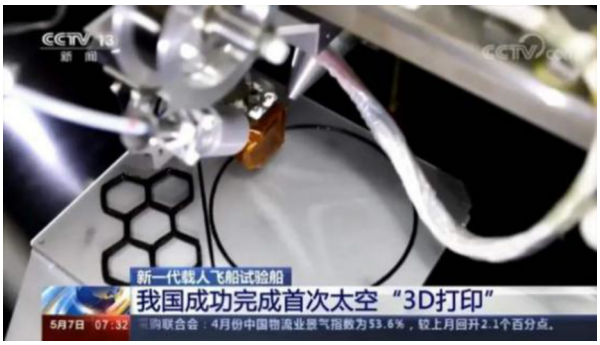

Fig. 20. First Chinese 3D-printing experiment in new-generation testing spacecraft with continuous fiber-reinforced composites.

In May 2020, a 3D printer for CFRTPCs was carried onboard a Chinese testing spacecraft to validate the printing process for composites, as shown in Fig. 20. Honeycomb composite structures were printed during the flight. This was not only the first Chinese 3D printing experiment in space, but also the first 3D printing of CFRTPCs in space.

4. Conclusions

The present work summarizes strategies for the development of AM technologies in space. In AM, processes, machines (technology), and materials are uniquely linked to each other. Therefore, it is a great challenge for scientists to develop appropriate AM technologies for space. Physical parameters such as gravitation, atmospheric pressure, and temperature in a laboratory are not easily adapted to simulate the space environment. The use of different platforms to simulate the space environment, from laboratory equipment to real-space missions, is discussed. The results obtained in parabolic flight campaigns, sounding rocket experiments, and re-entry missions are highlighted, and it is demonstrated that the use of appropriate platforms can help to progress development. However, there are limitations in the iteration speed of the experiments and the total time. For example, the microgravity environment significantly restricts the speed of development. For the effective use of different space simulating platforms, it is necessary to clarify the impacts of each physical parameter on the properties of the material, production process, and technology. For instance, missing gravitation has a limited effect on the material, but has strong effects on process and technology. In contrast, the vacuum has a limited effect on the process and technology, but has a significant effect on the material. A better understanding of these relations, one-by-one, would help in effectively designing experiments and choosing the appropriate platforms.

Declaration of Competing Interest

The authors declare that they have no known competing financial interests or personal relationships that could have influenced the work reported in this paper.

CRediT authorship contribution statement

Andrea Zocca: Writing – review & editing. **Janka Wilbig:** Writing – review & editing. **Anja Waske:** Writing – review & editing. **Jens Günster:** Conceptualization, Writing – review & editing. **Martinus Putra Widjaja:** Writing – review & editing. **Christian Neumann:** Writing – review & editing. **Mélanie Clozel:** Writing – review & editing. **Andreas Meyer:** Writing – review & editing. **Jifeng Ding:** Writing – review & editing. **Zuoxin Zhou:** Writing – review & editing. **Xiaoyong Tian:** Writing – review & editing.

Acknowledgments

The authors thank ESA and Novespace for their support in the 76th ESA parabolic flight campaign, and DLR and Novaspace for their support in DLR parabolic flight campaigns 30, 31, 33, 34, and 36.

The authors thank Marcel Grunwald (BAM 8.3) for technical support with the X-ray computed tomography scan. We gratefully acknowledge the Swedish Space Corporation for hosting and supporting the research teams during the MAPHEUS rocket launch campaign.

References

[1] Fateri M, Meurisse A, Sperl M, et al. Solar sintering for lunar additive manufacturing. J Aerosp Eng 2019;32(6):0001093.
[2] Pletser V, Rouquette S, Friedrich U, et al. European parabolic flight campaigns with Airbus ZERO-G: Looking back at the A300 and looking forward to the A310. Adv Space Res 2015;56(5):1003–13.
[3] Kirchhartz R, Hörschgen-Eggers M, Jung W. Sounding rockets are unique experimental platforms. 69th International Astronautical Congress; 2018. 01- 05 OctBremen, Germany.
[4] Wainscott-Sargent A. The New Gold Rush: 3D Printing in Micro-G. (June 26, 2017). https://www.issnationallab.org/iss360/the-new-gold-rush-3d-printing-in-micro-g.
[5] Labeaga-Martínez N, Sanjurjo-Rivo M, Díaz-Álvarez J, et al. Additive manufacturing for a Moon village. In: Procedia Manufacturing, 13; 2017. p. 794–801.
[6] Goulas A, Engstrøm D S, Friel R J. Additive manufacturing using space resources. Handbooks in Advanced Manufacturing: Additive Manufacturing, Amsterdam:Elsevier 2021.
[7] Karl D, Duminy T, Lima P, al et. Clay in situ resource utilization with Mars global simulant slurries for additive manufacturing and traditional shaping of unfired green bodies. Acta Astronaut 2020;174:241–53.
[8] Jakus A E, Koube K D, Geisendorfer N R, al et. Robust and elastic lunar and martian structures from 3D-printed regolith inks. Sci Rep 2017;7:44931.
[9] Cesaretti G, Dini E, De Kestelier X, et al. Building components for an outpost on the Lunar soil by means of a novel 3D printing technology. Acta Astronaut 2014;93:430–50.
[10] Fateri M, Pitikaris S, Sperl M. Investigation on wetting and melting behavior of lunar regolith simulant for additive manufacturing application. Microgravity Sci Technol 2019;31(2):161–7.
[11] Balla V K, Roberson L B, O'Connor G W, et al. First demonstration on direct laser fabrication of lunar regolith parts. Rapid Prototyping J 2012:20110000850.
[12] Fateri M, Gebhardt A. Process parameters development of selective laser melting of lunar regolith for on-site manufacturing applications. Int J Appl Ceram Technol 2015;12(1):46–52 1.
[13] Fateri M, Meurisse A, Sperl M, et al. Solar sintering for lunar additive manufacturing. J Aerosp Eng 2019;32(6):0001093.
[14] Reitz B, Lotz C, Gerdes N, al et. Additive manufacturing under lunar gravity and microgravity. Microgravity Sci Technol 2021;33:25.
[15] Zocca A, Lüchtenborg J, Mühler T, et al. Enabling the 3D printing of metal components in μ-gravity. J Mater Process Technol 2019;4(10):1900506.
[16] Baldemar P, Widell O. The Esrange facility in northern Sweden-your partner for successful aerospace operations. AIP Conf Proc 2002;609:239–42.
[17] Kargl F, Drescher J, Dreißigacker C, al et. XRISE-M: X-radiography facility for solidification and diffusion studies of alloys aboard sounding rockets. Rev Sci Instrum 2020;91:013906.
[18] Tell K, Dreißigacker C, Tchapnda A C, et al. Acoustic waves in granular packings at low confinement pressure. Rev Sci Instrum 2020;91:033906.
[19] Bräuer D, Neumann C. Camera-based sample-position detection and control for microgravity electrostatic levitation. Rev Sci Instrum 2020;91:043904.
[20] Keßler R, Bräuer D, Dreißigacker C, et al. Direct-imaging of light-driven colloidal Janus particles in weightlessness. Rev Sci Instrum 2020;91:013902.
[21] Balter M, Neumann C, Bräuer D, et al. ARTEC—A furnace module for directional solidification and quenching experiments in microgravity. Rev Sci Instrum 2019;90:125117.
[22] Sondermann E, Jakse N, Binder K, et al. Concentration dependence of interdiffusion in aluminum-rich Al-Cu melts. Phys Rev B 2019;99:024204.
[23] Siegl M, Kargl F, Scheuerpflug F, et al. Material physics rockets MAPHEUS-3/4: flights and developments. In: Proceedings of the 21st ESA Symposium on European Rocket and Balloon Programmes and Related Research. 21st ESA Symposium on European Rocket and Balloon Programmes and Related Research; 2013. p. 9–13. JunThun, Schweiz.
[24] Stamminger A, Ettl J, Blochberger G, et al. MAPHEUS-1: Vehicle, subsystem design, flight performance and experiments. In: Proceedings of the 19th ESA Symposium on European Rocket and Balloon Programmes and Related Research, Seiten 411-416. ESA Communication Production Office. 19th ESA Symposium on European Rocket and Balloon Programmes and Realted Research; 2009. p. 7–11. JunBad Reichenhall, Deutschland.
[25] Steinbach S, Ratke L. Effects of controlled convections on dendritic microstructure and segregation during microgravity-solidification. In: Proc. 18th ESA Symposium on European Rocket and Balloon Programmes and Related Research; 2007.
[26] Nguyen-Thi H, Reinhart G, Billia B. On the interest of microgravity experimentation for studying convective effects during the directional solidification of metal alloys. Comptes Rendus Mécanique 2017;345(1):66–77.

[27] Li X P, Roberts M P, O'Keeffe S, et al. Selective laser melting of Zr-based bulk metallic glasses: processing, microstructure and mechanical properties. Mater Design 2016;112:217–26.
[28] Ouyang D, Li N, Xing W, et al. 3D printing of crack-free high strength Zr-based bulk metallic glass composite by selective laser melting. Intermetallics 2017;90:128–34.
[29] Best J P, Ast J, Li B, et al. Relating fracture toughness to micro-pillar compression response for a laser powder bed additive manufactured bulk metallic glass. Mater Sci Eng 2020;770:138535.
[30] Yang C, Tian X, Li D, et al. Influence of thermal processing conditions in 3D printing on the crystallinity and mechanical properties of PEEK material. J Mater Process Technol 2017;248:1–7.
[31] Tian X, Liu T, Yang C, et al. Interface and performance of 3D printed continuous carbon fiber reinforced PLA composites. Compos Part A 2016;88:198–205.
[32] Tian X, Liu T, Wang Q, et al. Recycling and remanufacturing of 3D printed continuous carbon fiber reinforced PLA composites. J Cleaner Prod 2017;142(4):1609–18.